journal

J. Am. Ceram. Soc., 83 [6] 1469–75 (2000)

Rate of Strength Decrease of Fiber-Reinforced Ceramic-Matrix Composites during Fatigue

Bent F. Sørensen

Materials Research Department, Risø National Laboratory, DK-4000 Roskilde, Denmark

John W. Holmes

Ceramic Composites Research Laboratory, Department of Mechanical Engineering and Applied Mechanics, The University of Michigan, Ann Arbor, Michigan 48109-2125

Eddy L. Vanswijgenhoven

Department of Metallurgy and Materials Engineering, Katholieke Universiteit Leuven, De Croylaan 2, B-3001 Heverlee, Belgium

An experimental investigation was performed to study the rate at which strength-controlling fatigue damage evolves in a ceramic-matrix composite. Tensile specimens of a unidirectional SiC-fiber-reinforced calcium aluminosilicate matrix composite were cycled to failure or to a preselected number of cycles under similar loading histories. The residual strength of the precycled specimens was found to be similar to that of virgin specimens. Microstructural investigations showed that the fracture surfaces of the specimens cycled to failure had a central region where fiber pullout was negligible. It is proposed that frictional heating (due to interfacial sliding) is the cause of fatigue failure. High interfacial temperatures are assumed to cause the formation of a strong interface bond, leading to internal embrittlement.

I. Introduction

Because of their damage-tolerant behavior, ceramic-matrix composites (CMCs) have the potential for use in high-temperature load-carrying components, such as turbine blades or heat exchangers. Before CMCs can be used in such applications, their long-term behavior under complex combinations of loads, temperatures, and environments must be understood.[1]

The monotonic stress–strain behavior of unidirectional composites has been studied extensively at room temperature.[2–4] The underlying damage mechanisms have been identified as the initiation and growth of multiple matrix cracks. The matrix cracks are bridged by intact fibers, with debonding and sliding occurring at the fiber/matrix interface. Composite failure occurs when the fibers fail. This distinction between matrix cracking and composite fracture provides damage-tolerant behavior; that is attractive from an engineering point of view. Models have been developed to describe these mechanisms.[5–8] The models predict that in order to have a damage-tolerant behavior, the interface bonding and sliding resistance must be sufficiently low, such that interfacial sliding can readily take place.

The stress–strain behavior of CMCs at high temperature may differ from the behavior observed at room temperature, since creep and oxidation damage may occur.[9–11] If oxidation occurs at the fiber/matrix interface, an interphase with strong bonding may form.[10,12,13] This hinders interfacial sliding, resulting in a loss of damage-tolerant behavior; the composite then fails in a brittle manner.

Most experimental studies of CMCs subjected to cyclic loading have been conducted at room temperature.[2,14–19] Typically, the composite stiffness decreases rapidly in the early cycles, reaching a minimum within 10^3–10^5 cycles.[15,17] The number of cycles to failure may be significantly higher than the number of cycles at which the modulus reaches a minimum.[17] Damage evolution during cyclic loading has been found to be similar to that found for monotonic tension (multiple matrix cracking, fiber/matrix debonding and sliding). In addition, during cyclic loading, repeated forward and reverse slip can occur at the fiber/matrix interface. Macroscopically, this slip results in hysteresis in the stress–strain behavior and a temperature rise of the specimens (frictional heating[16,17,20]). At the microscale, cyclic slip may result in interfacial wear,[17,19,21] lowering the interfacial frictional sliding shear stress, τ. It has been proposed that a decrease in the interfacial shear stress may decrease the composite strength and cause fatigue failure.[19] For instance, for 2D SiC/SiC, Rouby and Reynaud[19] found a fatigue limit (maximum allowable stress, σ_{max} giving run-out) at 2.5×10^5 cycles, which corresponded nicely with predictions based on a decrease in τ. In their study, fatigue failures all occurred within 2×10^4 cycles. This is consistent with the decrease in τ, which occurs within a low number of cycles. Thus, for high stresses, a mechanism for low cycle fatigue failure appears to be the cyclic-induced decrease in τ. However, for other CMCs, the number of cycles to failure can exceed by orders of magnitude the number of cycles at which the interfacial shear stress reaches a minimum value.[17,20,22] This disparity suggests that additional fatigue damage mechanisms exist.

Experimental fatigue studies conducted at high temperature have shown that embrittlement due to oxidation damage of the interphase layer may be the most severe problem.[10,23–26] Holmes[27] found that the life of cyclically loaded SCS-6 SiC_f/Si_3N_4 specimens at 1200°C was shorter than the creep life. The fatigue life decreased with decreasing stress ratio. This provides clear evidence of a high-temperature fatigue-life controlling mechanism. Thus, fatigue interactions with oxidation and creep are damage mechanisms that must be understood.

F. W. Zok—contributing editor

Manuscript No. 189843. Received September 30, 1998; approved December 14, 1999.

Support for B. F. Sørensen was provided by the Risø Engineering Science Center for Structural Characterization and Modeling of Materials. Additional support was provided by the National Science Foundation (Grant No. DMR-9257557) and the Air Force Office of Scientific Research (Grant No. F49620-95-1-0206).

*Member, American Ceramic Society.

Fatigue failure occurs when the residual strength of the composite, σ_u, has decreased to the maximum applied cyclic stress, σ_{max}. It is the aim of the present study to investigate the rate at which the strength-controlling damage evolves in a CMC during high cycle fatigue at room temperature. The experimental approach is straightforward. The tensile strength of virgin and prefatigued specimens is determined experimentally. Other specimens are cycled under similar conditions until fatigue failure occurs. Then, a diagram of composite strength as a function of number of load cycles can be constructed.

II. Experimental Methods

(1) Specimen Preparation

The material used in this study was an 8-ply unidirectional Nicalon SiC-fiber-reinforced calcium aluminosilicate composite, denoted SiC_f/CAS II, from Corning Inc. The nominal fiber volume fraction was 35–40%. The composite was processed by hot pressing. During processing, an approximately 0.1 μm thick carbon-rich interphase layer developed around the SiC fibers[12,13] (The thickness of the carbon layer, which depends on processing conditions, was not measured in the present study.) The carbon-interphase layer is known to enable debonding and frictional sliding along the interfaces. The fiber diameters were in the range of 10–20 μm.

Edge-loaded tensile specimens,[28] with the tensile direction parallel with the fiber direction, were cut from rectangular plates. A minor face of each specimen was polished to allow the matrix crack spacing to be measured. The polishing was performed using a 38 mm mandrel rotating at 1500 rpm. The following polishing procedure was used: (1) 600-grit SiC paper for 5 min, (2) 45 μm diamond paste for 5 min (nylon cloth), (3) 6 μm diamond paste for 5 min (nylon cloth), (4) 1.0 μm diamond paste for 10 min (nylon cloth).

(2) Mechanical Testing

Four specimens were loaded in monotonic uniaxial tension (the loading rate was 100 MPa/s) to establish the stiffness and strength of the virgin material. Four other specimens were cycled under identical conditions (σ_{max} = 240 MPa, σ_{min} = 10 MPa, 200 Hz) until fatigue failure occurred. Four additional specimens were cycled under the same conditions, but for only 10^5 cycles, which was slightly lower than the number of cycles to failure found for the previous samples. These specimens were then loaded in monotonic tension (100 MPa/s) in order to measure the residual strength of the composite after 10^5 cycles.

All fatigue experiments were conducted on a MTS servohydraulic test frame (Model No. 331, MTS Systems Corp., Minneapolis, MN). The fatigue tests were performed inside a 0.1 m^3 water-cooled chamber, where the temperature of the walls and grips was kept constant at 22.0 ± 0.1°C (see Holmes and Cho[17] for details). The temperature rise of the specimen surface (caused by frictional heating) was measured with an infrared pyrometer (Model No. 5402, Everest Interscience Inc., Fullerton, CA), focused at a 5 mm spot size within the specimen gauge section. In order to achieve stable temperature conditions, the chamber temperature was allowed to stabilize for at least 2 h before the fatigue tests were started. The axial strain data were measured with an extensometer (Model 632.27B-20, MTS System Corp.) with a 33 mm gauge length. For the cyclic tests, the extensometer was mounted along a specimen edge by O-rings and fixed to the specimen with Super-Glue. Stress–strain data were recorded at regular intervals, and from these data the hysteresis modulus (averaged over one cycle) was calculated as a function of the number of load cycles.

The specimens were cycled between σ_{min} = 10 MPa and σ_{max} = 240 MPa with a sinusoidal waveform at a frequency of 200 Hz. In order to prevent overshooting during the first few load cycles, the load span was increased (linearly with time) from zero to the maximum stress within 0.8 s.

(3) Microstructural Characterization

After the tensile or fatigue tests, the average matrix crack spacing was measured at the polished face by optical microscopy (prior work had shown that well-developed surface cracks typically span the entire cross section of a specimen), as follows: The number of cracks was counted along 20–30 mm long lines parallel with the fiber direction. Usually more than 300 cracks were counted. All measurements were taken away from the localized region associated with the fracture surface. Fracture surfaces were inspected with optical and environmental scanning electron microscopes (Model E-3, ElectroScan Corp., Wilmington, MA). In order to observe debris at the fracture surfaces, the specimens were neither cleaned nor coated before being investigated. Finally, using a conventional scanning electron microscope, overview pictures were taken of gold-coated fracture surfaces.

III. Results and Discussion

(1) Monotonic Tensile Tests of Virgin Specimens

Typical stress–strain curves for the virgin material are shown in Fig. 1. The shape of the stress–strain curves is typical of damage-tolerant CMCs.[3,4,17] The shape reflects elastic response at low strain (stage I), multiple matrix cracking (stage II), large-scale interfacial slip along the interfaces of intact fibers (stage III), and distributed fiber failures (stage IV) prior to localization of damage. Some characteristic parameters of the virgin composite are summarized in Table I. E_c is the elastic modulus within the first linear portion of the stress–strain curve, $\sigma_{0.02}$ is the stress level where the axial strain, ε, deviates 0.02% from linear elasticity (note that matrix cracks develop below $\sigma_{0.02}$[3,4]), σ_u and ε_u are the failure stress and strain, respectively, and s is the average matrix crack spacing measured after the tensile test. The fiber volume fraction, v_f, was calculated by the rule of mixtures, utilizing a Young's modulus of 200 and 98 GPa, respectively, for the fibers and matrix.[3,4] A similar value of v_f was found by the area fraction method (i.e., by using micrographs to estimate the cross-sectional area fraction of fibers).

For all specimens, the fracture was located within the gage section. The fracture surface was macroscopically flat, but displayed considerable fiber pull-out (Fig. 2). In the region near the fracture surface, the matrix cracks were opened significantly more than at locations distant to the fracture site. This enhanced crack opening is assumed to have occurred by fibers that had broken and subsequently pulled out. Thus, the length of this localization zone, L (Table I), is an indirect measure of the interfacial sliding shear stress.

(2) Specimens Cycled to Failure

The shape of the cyclic stress–strain curves changed during cycling. These changes were accompanied by the development of a permanent offset strain, ε*, and an increase in the surface

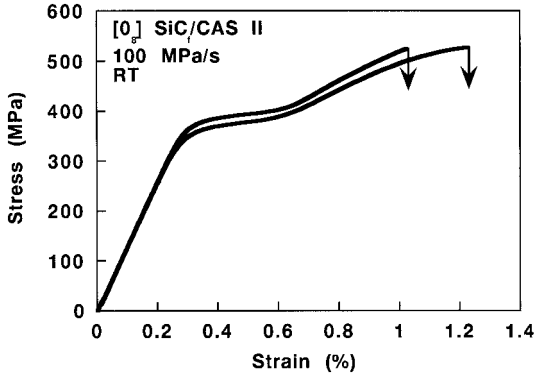

Fig. 1. Two typical monotonic stress–strain curves obtained from virgin specimens.

Table I. Summary of Monotonic Tensile Test Results

E_c	133.7 ± 3.4 GPa
$\sigma_{0.02}$	351 ± 8 MPa
σ_u	508 ± 31 MPa
ε_u	1.05 ± 0.17%
s	154 ± 17 μm
v_f	0.35 ± 0.03
L	≈0.4 mm

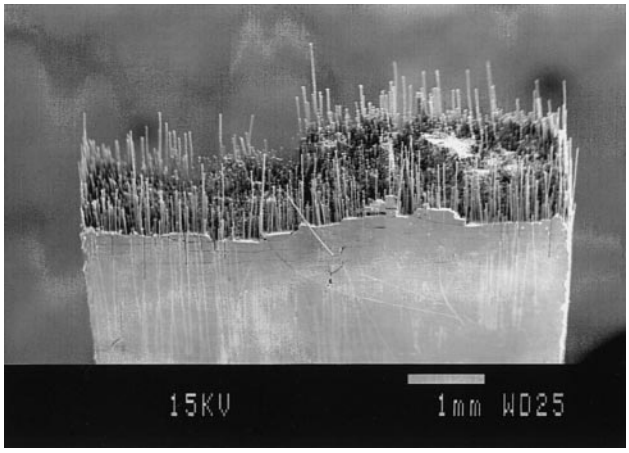

Fig. 2. SEM micrograph showing the fracture surface of a specimen tested in monotonic tension.

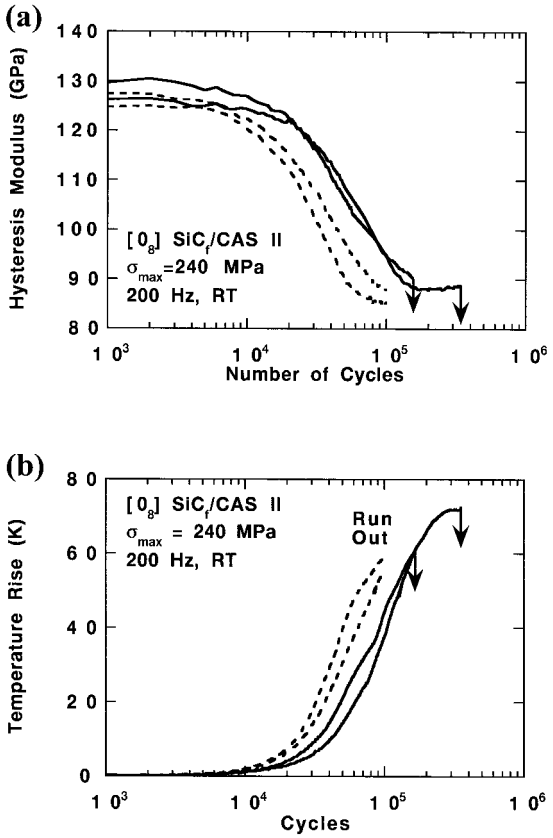

Fig. 3. Recorded damage indicators for two typical specimens cycled to failure (solid lines) and specimens cycled to 10^5 cycles (dashed lines): (a) evolution of the hysteresis modulus as a function of the number of load cycles N; (b) temperature rise, ΔT, as a function of the number of cycles.

temperature, ΔT, of the specimen (due to frictional energy dissipation).

The hysteresis modulus, $\bar{E}$, was calculated from the stress–strain data. Figure 3(a) shows how $\bar{E}$ changes as a function of the number of cycles N for specimens that were cycled to failure. The evolution of $\bar{E}$ for all four specimens follows the same trend: The modulus decreases significantly, to about 87 GPa within approximately 2×10^5 cycles. Thereafter $\bar{E}$ remains nearly constant (a slight modulus recovery, about 1 GPa, was found for two of the specimens).

Values for the characteristic parameters are listed in Table II. Note that the values of $\bar{E}$ and ε^* are the values that were measured just before localization occurred; s was measured away from the localized region after fatigue failure. These parameters can thus be used in micromechanical models, which are based on intact fibers.

Figure 3(b) shows the temperature rise curves recorded for the specimens cycled to failure. For these specimens fatigue failure occurred outside the 5 mm spot size of the infrared pyrometer. The heating curves follow the same trend; they increased slowly within the first 10^4 cycles, but increased rapidly during additional cycling. This rapid increase is attributed to an increasing number of matrix cracks and accompanying slip zones. The peak temperatures of the four specimens differ somewhat. This difference is attributed to the fact that the specimens fail at different numbers of cycles, while the temperature is increasing. If they had failed at the same number of cycles, the maximum temperature rise of each specimen likely would have been roughly the same. For specimens that failed within the spot size of the pyrometer a very rapid temperature rise occurred within the last few seconds before failure.

The fracture surfaces of the specimens cycled to failure had two distinctively different regions. One part of the fracture surface displayed fiber pull-out, while the other area had no fiber pull-out (Fig. 4). The area without fiber pull-out was located in the core of the specimen cross section; fiber pull-out was always present in a region near the specimen edges. This appearance is opposite to that found at the fracture surfaces of specimens that have been exposed to external oxidation.[11] The appearance of the fracture surface (Fig. 4(a)) suggests that the center region failed before final overload of the remainder cross section. At some locations (within the core region with no fiber pull-out) significant debris was present (Fig. 4(b)).

Table II. Characteristics of Specimens Cycled to Failure

$\bar{E}$	87 ± 7 GPa
ε^*	0.08 ± 0.01%
s	144 ± 33 μm
L	≈1.0 mm
N_f	1.3×10^5–3.5×10^5
$(\Delta T)_{max}$	69 ± 14 K

Like the fracture surface, the broad faces of the specimens were found to have an inhomogeneous appearance. Along the sides of the specimens there were zones with larger matrix crack openings (Fig. 5). The length (in the fiber direction) of this localized zone, L, was about 6–10 times the matrix crack spacing. This is considerably larger than the localized zone found after monotonically loading virgin specimens to failure (see Table I). The larger L of the cyclically loaded specimens indicates a lower value of τ. In contrast, in the middle of the broad face (where the core region was close to the surface), there was no such localized zone; the matrix crack opening was similar to that remote from the fracture site. This indicates that no global load sharing and no fiber pull-out had taken place near the core region during specimen failure.

(3) Specimens Cycled to 10^5 Cycles

The evolution of hysteresis modulus and the temperature rise of specimens cycled to 10^5 cycles are included in Fig. 3. After

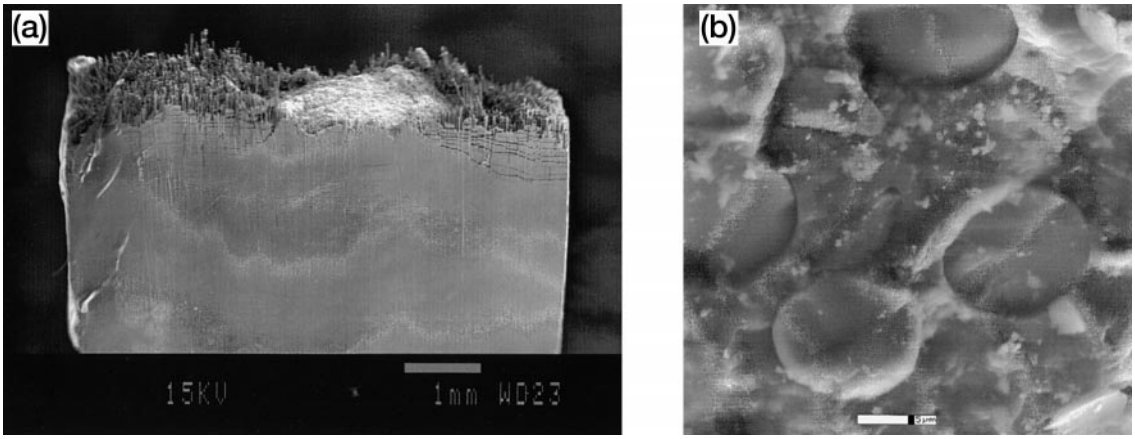

Fig. 4. Micrographs showing part of the fracture surface of a typical specimen cycled to fatigue failure: (a) overview (conventional SEM), showing the core region without fiber pull-out and the external region with extensive pull-out; (b) ESEM micrograph of the core region with no fiber pull-out, but debris at the fibers and matrix.

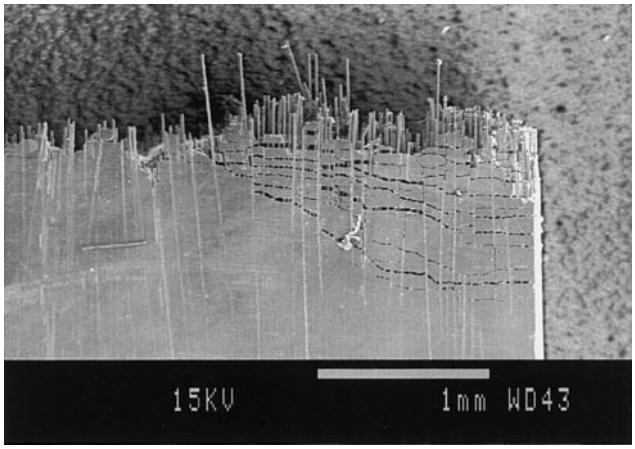

Fig. 5. Micrograph of the broad face of a specimen cycled to failure. Near the edge there is a zone where the fiber pull-out has caused larger crack openings. The length of this zone, L, is about 8–10 crack spacings. In the center of the specimens (close to the core region) such a zone is absent.

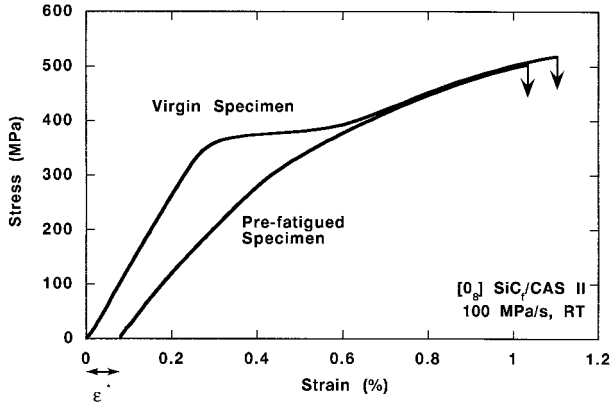

Fig. 6. Comparison between the stress–strain behavior of a virgin specimen and the tensile curve of a precycled specimen. The stress–strain curve of the precycled specimen is offset by the permanent strain, ε*, that was recorded at zero load after cycling. The two curves are very similar for stresses above the matrix crack saturation of the virgin specimen.

cycling, the specimens had a permanent strain, ε*. The average matrix crack spacing was measured after cycling and after the tensile tests (Table III). $\bar{E}$ was measured from the stress–strain data (0–0.2% axial strain) obtained from the residual strength test, and the interfacial shear stress τ was calculated from models[29–31] using the approach described in the Appendix. The value of τ at 10^5 cycles (6 MPa) is roughly similar to the value derived from frictional heating experiments,[17,22] but significantly lower than the value for the virgin composite, which is typically about 20–30 MPa.[17,32–34] This confirms the hypothesis that τ decreases during cycling (note, however, that τ may be velocity dependent[34,35]).

A typical tensile curve for a specimen cycled to 10^5 cycles is plotted in Fig. 6, together with a stress–strain curve for the virgin material. In order to obtain a true comparison, the strain value of the prefatigued specimen is offset by a value ε*, which is the permanent strain that was recorded at the unloaded state after cycling. While the monotonic tensile curve of the virgin specimen exhibits linear elastic behavior at low applied stress, the tensile curve of the prefatigued specimen is nonlinear even at low loads. This nonlinearity is attributed to the fact that the precycled specimens possess significant damage (distributed matrix cracking and interfacial debonding) prior to the tensile test, while the virgin material is free of damage. Beyond 400 MPa (assumed to be the stress level corresponding to matrix crack saturation) the two curves follow each other closely. This indicates that the damage states of the virgin and precycled specimens are very similar at these stress levels. Indeed, the average matrix crack spacing was 154 ± 10 μm for the virgin specimens (after the tension test) and 156 ± 10 μm for the specimens cycled to 10^5 cycles (after cycling), and 112 ± 10 μm after the residual strength tests. The residual strength of the prefatigued specimens was 491 ± 13 MPa (Table III). Thus, both the matrix crack spacing and the composite strength of the prefatigued specimens were fairly similar to those of the virgin specimens.

The fracture surface of the prefatigued specimens had a large amount of fiber pull-out (see Fig. 7). Unlike the specimens cycled to failure, the prefatigued specimens showed fiber pull-out over the entire fracture surface. The pull-out length of the precycled specimens is significantly longer than for the virgin specimens (compare Figs. 2 and 7). The length of the localized zone, L, was also longer than for the virgin specimens. Both of these results

Table III. Characteristics of Specimens Cycled to 10^5 Cycles

$\bar{E}$	91.3 ± 1.5 GPa
ε*	0.07 ± 0.01%
s	156 ± 10 μm (112 ± 10 μm)[†]
L	≈0.8 mm
σ_u	491 ± 13 MPa
τ	6.0 ± 0.7 MPa
$(\Delta T)_{max}$	63 ± 3 K

[†]Value of s in parentheses refers to the value measured after the tensile test.

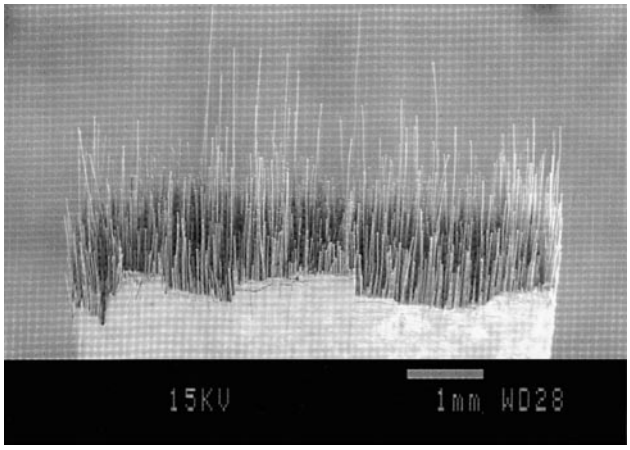

Fig. 7. SEM micrographs of a typical fracture surface of a specimen cycled to 10^5 cycles and tested in monotonic tension thereafter.

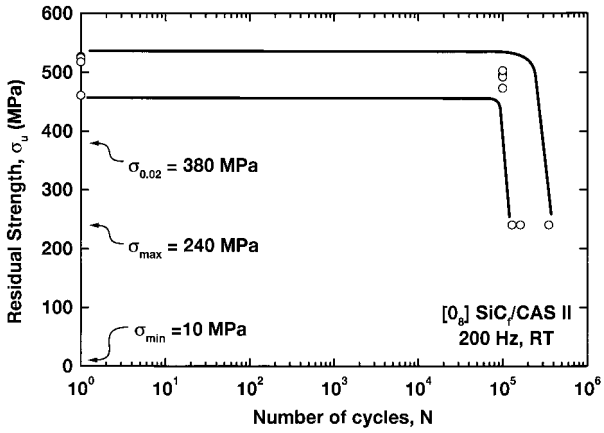

Fig. 8. Residual composite strength as a function of the number of load cycles. The residual strength is fully retained at approximately 500 MPa until 10^5 cycles, but decreases to 240 MPa within a short number of cycles thereafter.

suggest that τ was lower for the precycled specimens than for the virgin material.

(4) Model Prediction of Residual Strength

Existing models for composite strength predict that a decrease in τ should result in a decrease in the residual strength.[8,19] These models are valid only if global load sharing (GLS) takes place; this requirement is fulfilled for specimens where fiber pull-out occurs across the entire fracture surface and the fiber pull-out length varies from one fiber to the next. These assumptions are fulfilled for the virgin specimens and the specimens cycled to 10^5 cycles. GLS models predict that the residual strength after N cycles, $\sigma_u(N)$, is related to the initial composite strength, σ_u^0, as[19]

$$\frac{\sigma_u(N)}{\sigma_u^0} = \left(\frac{\tau(N)}{\tau^0}\right)^{1/(m+1)} \tag{1}$$

where τ^0 is the initial value of τ, $\tau(N)$ is the value attained after N cycles, and m is the Weibull modulus describing the strength variation of the fibers (in Eq. (1) the fiber strength is assumed to remain unchanged during cycling). Equation (1) predicts that if τ decreases during cycling ($\tau(N) < \tau^0$), then the residual strength of the composite decreases as well. Using $\tau = 20$ MPa, $\tau(N=10^5) = 6$ MPa, $m = 3$ (value taken from Curtin[8]), $\sigma_u^0 = 508$ MPa (Table I), Eq. (1) predicts $\sigma_u(N=10^5) = 376$ MPa. This prediction is significantly lower than the experimental results (491 MPa, Table II). This inconsistency indicates that a decrease in the interfacial shear stress, acting alone, may not have the effect predicted by the GLS models, and that the models do not adequately describe the high cycle fatigue failure of CMCs.

(5) Residual Strength as a Function of Cycles

From the measured strength values a graph that shows the residual strength of the composite as a function of the number of cycles can be constructed. The four specimens that were cycled to failure are also included in this graph, since the residual strength of these specimens must have been equal to σ_{max} (i.e., 240 MPa) when they failed. The results are presented in Fig. 8. As already mentioned the residual strength of the specimens cycled for 10^5 cycles was almost the same as that measured for the virgin specimens. From Fig. 8, we conclude that the loss of composite strength does not occur gradually over the fatigue life; *rather, for this unidirectional composite, the loss of residual strength of the composite occurs within the last 20% of the specimen lifetime.*

It should be noted that although the present results are obtained at specific test conditions, similar results have been found under different conditions.[36] Therefore, the trends of the results are likely to be of a general nature.

IV. A Possible High Cycle Fatigue Damage Mechanism

(1) Summary of Observed Behavior

There are several characteristic features of the high-frequency fatigue process:

(1) The temperature of the specimen increases during the initial stages of fatigue. Next, it levels off and, for long-duration fatigue at moderate stress levels, decreases. If failure is avoided, the shape of the temperature rise curve is often bell shaped. If failure occurs, a sharp rise in temperature occurs within the localized zone immediately prior to fracture (typically of the order of several seconds).

(2) The density of matrix cracks increases rapidly during the initial stages of fatigue. For a fixed maximum stress, this crack density quickly stabilizes and remains constant for the duration of the fatigue life. The development of matrix cracks is assumed to be influenced by stress corrosion cracking[37] and decrease in τ due to interfacial wear.[17]

(3) The hysteresis modulus decreases rapidly during the initial stages of fatigue, reaches an approximate plateau, and, if failure is avoided, may show a gradual increase. The initial modulus decrease is attributed to the formation of matrix cracks and a decrease in τ; the later modulus recovery is likely to be caused by an increase in τ. The increase in τ may be caused by various mechanisms, such as accumulation of debris along the interface or a chemical reaction, increasing the interfacial sliding resistance or bonding.

(4) A unique feature of high cycle fatigue failure is the formation of a central zone where the fiber pull-out lengths are negligible. Surrounding this zone, which consumes roughly half of the fracture surface, is a zone of extensive fiber pull-out. Specimens that were prefatigued at the same stress level, followed by monotonic loading to failure, exhibited extensive fiber pull-out throughout the entire fracture surface. Virgin specimens tested under monotonic tension also exhibited nearly uniform fiber pull-out across the entire fracture surface.

(2) Interpretation of Fracture Surface and Failure Mode

Since the fracture surface of the prefatigued specimens exhibited extensive fiber pull-out, the central core (in specimens cycled to failure) must have formed very rapidly just prior to specimen fracture (between 10^5 cycles and the occurrence of fatigue failure). To understand the development of the core region, we must identify a mechanism that can form a region with no fiber pull-out within a short number of cycles. Apparently the final stage (localization) is not cycle count dependent but damage and temperature rise dependent.

The lack of fiber pull-out in the core region indicates that the usual composite behavior (interfacial slip) has been hindered,

either by an increase in the interfacial shear stress or by the formation of strong interface bonding. If global load sharing cannot occur, the composite behaves like a brittle material in the core; matrix cracking can penetrate the fibers.

But why has the damage developed differently in the center of the cross section than at the edges? The answer is not obvious, since for 1D composites the macroscopic stress state (uniaxial tension) does not vary across the cross section. Other parameters may vary across the cross section, such as humidity, oxygen concentration, and temperature field. The latter may vary across the specimen cross section, since energy is lost at the surface by radiation and convection.

(3) A Fatigue Damage Mechanism: Embrittlement Due to Internal Heating

Assume that the interfacial shear stress can increase or a strong bonding can form with increasing temperature and time. Next, imagine a situation where composite cross section (in the localized region) consists of three domains (see Fig. 9): The core area (domain I), in which the fibers are broken (initially, there may be no broken fibers in domain I; it may start from a crack in a matrix-rich region). Outside the core area is a transition zone (domain II) where the stresses at the fibers are now higher than the nominal value, since there is local load sharing (stress concentration), and domain III, where intact fibers experience global load sharing due to a lower value of τ.

Fatigue damage may evolve as follows. During cyclic loading the energy dissipation is highest in domain II, near the fibers located at the edge of domain I (at this location the fibers experience the highest stress concentration). If the resulting temperature rise is sufficiently high, then after some time interfacial slip may be hindered and the fibers in the vicinity of domain I fail, transferring more stress on the surviving fibers in domain II. These fibers are now subjected to the highest stresses and temperature. In this manner, domain I can extend across the cross section of the specimen; the mechanism is self-sustaining. The composite fails when the remaining cross section cannot carry the maximum applied load. Then the fracture surface will show an interior region with no fiber pull-out (corresponding to domain I), a transition region with short fiber pull-out lengths (domain II), and an exterior region displaying usual fiber pull-out (note that shorter fiber pull-out lengths reflect a higher interfacial shear stress[8]). The predicted appearance of the fracture surface is consistent with the observations in Figs. 4 and 5.

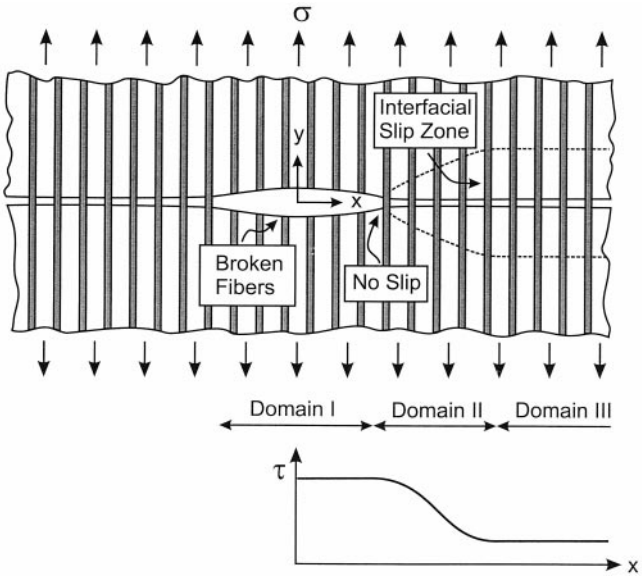

Fig. 9. Schematic drawing of the proposed fatigue damage mechanism. Fibers fail when the interfacial shear stress becomes so high that fiber/matrix slip is hindered. The assumed variation of the interfacial shear stress is indicated.

It is plausible that it may take a certain temperature and time before the interface damage reaches the critical state, where fiber slip can no longer occur. Thus, in the initial stages, fatigue damage may increase slowly, without causing fiber failures.

The fatigue mechanism postulated above may in principle explain the following experimental observations:

(1) A larger stress range and higher loading frequency shorten the fatigue life of CMCs with weakly bonded interfaces.[20,38] This may be understood in terms of the local temperature at the fiber/matrix interface, which may scale roughly with the energy dissipation.[22] Both a larger stress range and a higher loading frequency increase the frictional energy dissipation (per unit time), resulting in a higher temperature rise. This may accelerate the increase in τ, and shorten the fatigue life.

(2) It has been found that thicker (32 ply) test specimens possess a lower fatigue life than thinner (8-ply) specimens.[39] The proposed fatigue mechanism indicates that the occurrence of fatigue failure will depend on geometry and the thermal boundary conditions. It is likely that, for identical loading conditions, thicker specimens possess a higher temperature rise in the center of the cross section than thinner specimens; temperature-induced damage is likely to progress at a faster rate.

(4) Temperature-Driven Interface Changes

The scenario described above is based on the assumption that the interfacial shear stress or bond decreases initially but then increases with increasing temperature and time. There may be several causes for changes in interfacial properties as the temperature increases. The test environment, such as humidity and oxygen, affects the sliding behavior of a CMC possessing a carbon interphase.[40,41] Obviously, such phenomena may depend on temperature. Probably the most documented phenomenon for embrittlement of CMCs is oxidation damage. If the temperature at the interface rises above approximately 200°C, the C-interphase layer may begin to disappear by oxidation to CO or CO_2 (see, e.g., Thomas and Sanches[42]). If the temperature at the interface exceeds about 700°C, the SiC fibers may decompose and form SiO_2 at the interface.[42] Since burn-off of the C-layer would reduce the mismatch between the fibers and matrix, it is likely that the interfacial shear stress τ decreases. On the other hand, the formation of SiO_2 results in strong bonding.[10,11,42] It is well known that strong interfacial bonding results in brittle behavior of CMCs.[14,23,25,42] It cannot be ruled out that fatigue failure may be caused by the formation of a strong SiO_2 bond (note that locally at contact points along the fiber/matrix interface, where the frictional energy dissipation takes place, the temperature may be much higher than the surrounding bulk temperature).

V. Conclusions

For the particular material system examined (8-ply unidirectional SiC_f/CAS II) and test conditions (room-temperature cycling between σ_{max} = 240 MPa and σ_{min} = 10 MPa at 200 Hz) the following were found:

(1) The residual strength of specimens cycled to 10^5 cycles was similar to the tensile strength of virgin specimens. Consequently, measurements of residual strength (e.g., after 10^5 cycles) cannot be used as a predictor of fatigue failure, since the strength decrease seems to take place only shortly before the occurrence of fatigue failure. Also, the retained strength raises doubts about the validity of GLS models, which predict a significant strength reduction if the interfacial shear stress decreases.

(2) The results suggest that frictional interface sliding was hindered within the specimen core, causing brittle fracture in the center of cross sections of the specimens.

APPENDIX

By the use of a simple micromechanical model τ can be computed from the hysteresis modulus, $\bar{E}$, or the stress–strain data from a monotonic tensile test of precycled specimens. For the latter, the following procedure is used. For a given strain increment from the unloaded state, $\Delta\varepsilon$, the corresponding stress increment, $\Delta\sigma$, is determined. The hysteresis modulus at that stress level is then $\bar{E} = \Delta\sigma/\Delta\varepsilon$. This value is then used in the model. However, different equations are valid for different states of interfacial slip. If the slip length is smaller than $s/2$ the composite experiences partial slip. Else, the composite experiences full slip. The transition between partial and full slip occurs when the hysteresis modulus is[31]

$$\bar{E}_{ps-fs} = \frac{E_c}{1 + \dfrac{1 - v_f}{v_f}\dfrac{E_m}{E_c}} \tag{A-1}$$

where E_m is the Young's modulus of the matrix. If $\bar{E} > \bar{E}_{ps-fs}$ the composite is in partial slip, and τ can be calculated from[29–31]

$$\tau = \frac{\bar{E}}{1 - \dfrac{\bar{E}}{E_c}}\frac{r}{s}\frac{\Delta\sigma}{E_f}\left(\frac{E_m}{E_c}\frac{1 - v_f}{v_f}\right)^2 \tag{A-2}$$

where E_f denotes the Young's modulus of the fiber and r is the fiber radius. If full slip applies ($\bar{E} < \bar{E}_{ps-fs}$), then τ can be calculated from[30,31]

$$\tau = \frac{\bar{E} - v_f E_c}{v_f \bar{E}}\frac{r}{s}\Delta\sigma \tag{A-3}$$

When $\bar{E}$ was determined from the stress–strain data of the residual strength test, the matrix crack spacing, s, recorded after cycling (i.e., before the tensile test) was used, since no additional matrix cracking is assumed to occur as long as the maximum applied stress is below the maximum stress level that was applied during the cycling.[17]

Acknowledgment

The impetus for this study arose from discussions with Dr. Xin Wu.

References

[1]J. W. Holmes and B. F. Sørensen, "Fatigue Behavior of Continuous-Fiber-Reinforced Ceramic Matrix Composites"; pp. 261–326 in *Elevated Temperature Behavior of Ceramic Matrix Composites*. Edited by S. V. Nair and K. Jakus. Butterworth Heineman, Newton, MA, 1995.

[2]P. Karandikar and T.-W. Chou, "Damage Development and Moduli Reductions in Nicalon–Calcium Aluminosilicate Composites under Static Fatigue and Cyclic Fatigue," *J. Am. Ceram. Soc.*, **76**, 1720–28 (1993).

[3]D. S. Beyerle, S. M. Spearing, F. W. Zok, and A. G. Evans, "Damage and Failure in Unidirectional Ceramic-Matrix Composites," *J. Am. Ceram. Soc.*, **75**, 2719–25 (1992).

[4]B. F. Sørensen and R. Talreja, "Analysis of Damage in Ceramic Matrix Composites," *Int. J. Damage Mech.*, **2**, 246–71 (1993).

[5]B. Budiansky, J. W. Hutchinson, and A. G. Evans, "Matrix Fracture in Fiber-Reinforced Ceramics," *J. Mech. Phys. Solids*, **34**, 167–78 (1986).

[6]L. N. McCartney, "Mechanics of Matrix Cracking in Brittle-Matrix Fiber-Reinforced Composites," *Proc. R. Soc. London*, **A409**, 329–50 (1987).

[7]Y. J. Weitsman and H. Zhu, "Multi-fracture of Ceramic Composites," *J. Mech. Phys. Solids*, **41**, 351–88 (1993).

[8]W. A. Curtin, "Theory of Mechanical Properties of Ceramic Matrix Composites," *J. Am. Ceram. Soc.*, **74**, 2837–45 (1991).

[9]J. W. Holmes and X. Wu, "Elevated Temperature Creep Behavior of Continuous Fiber-Reinforced Ceramics"; pp. 193–260 in *Elevated Temperature Behavior of Ceramic Matrix Composites*. Edited by S. V. Nair and K. Jakus. Butterworth Heineman, Newton, MA, 1995.

[10]L. Filipuzzi, G. Camus, R. Naslain, and J. Thébault, "Oxidation Mechanisms and Kinetics of 1D-SiC/C/SiC Composite Materials: I, An Experimental Approach," *J. Am. Ceram. Soc.*, **70**, 459–66 (1996).

[11]A. G. Evans, F. W. Zok, R. M. McMeeking, and Z. Z. Du, "Models of High-Temperature, Environmentally Assisted Embrittlement in Ceramic Matrix Composites," *J. Am. Ceram. Soc.*, **79**, 2345–52 (1996).

[12]R. F. Cooper and K. Chyung, "Structure and Chemistry of Fiber-Matrix Interfaces in Silicon Carbide Fiber-Reinforced Glass-Ceramic Composites: An Electron Microscopy Study," *J. Mater. Sci.*, **22**, 3148–69 (1987).

[13]L. A. Bonney and R. F. Cooper, "Reaction Layer Interfaces in SiC-Fiber-Reinforced Glass-Ceramics: A High-Resolution Scanning Transmission Electron Microscopy Analysis," *J. Am. Ceram. Soc.*, **73**, 2916–26 (1990).

[14]K. M. Prewo, "Fatigue and Stress Rupture of Silicon Carbide Fiber-Reinforced Glass-Ceramics," *J. Mater. Sci.*, **22**, 2695–701 (1987).

[15]L. M. Butkus, L. P. Zawada, and G. A. Hartman, "Room Temperature Tensile and Fatigue Properties of Silicon Carbide Fiber-Reinforced Ceramic Matrix Composites"; in *Aeromat'90, Advanced Aerospace Materials/Processes Conference* (Long Beach, CA, May 21–24, 1990), 1990.

[16]J. W. Holmes and S. F. Shuler, "Temperature Rise During Fatigue of Fiber-Reinforced Ceramics," *J. Mater. Sci. Lett.*, **9**, 1290–91 (1990).

[17]J. W. Holmes and C. Cho, "Experimental Observations of Frictional Heating in Fiber-Reinforced Ceramics," *J. Am. Ceram. Soc.*, **75**, 929–38 (1992).

[18]L. P. Zawada, L. M. Butkus, and G. A. Hartman, "Room Temperature Tensile and Fatigue Properties of Silicon Carbide Fiber-Reinforced Aluminosilicate Glass," *Ceram. Eng. Sci. Proc.*, **11**, 1592–606 (1990).

[19]D. Rouby and P. Reynaud, "Fatigue Behavior Related to the Interface Modification during Load Cycling in Ceramic-Matrix Composites," *Compos. Sci. Technol.*, **48**, 109–18 (1993).

[20]J. W. Holmes, X. Wu, and B. F. Sørensen, "Frequency Dependency of Fatigue Life and Internal Heating of a Fiber-Reinforced Ceramic Matrix Composite," *J. Am. Ceram. Soc.*, **77**, 3284–86 (1994).

[21]A. G. Evans, F. W. Zok, and R. M. McMeeking, "Fatigue of Ceramic Matrix Composites," *Acta Metall. Mater.*, **43**, 859–75 (1995).

[22]C. Cho, J. W. Holmes, and J. R. Barber, "Estimation of Interfacial Shear in Ceramic Composites from Frictional Heating Measurements," *J. Am. Ceram. Soc.*, **74**, 2808–18 (1991).

[23]E. Y. Luh and A. G. Evans, "High-Temperature Mechanical Properties of a Ceramic Matrix Composite," *J. Am. Ceram. Soc.*, **70**, 466–69 (1987).

[24]K. M. Prewo, B. Johnson, and S. Starrett, "Silicon Carbide Fibre-Reinforced Glass-Ceramic Composite Tensile Behaviour at Elevated Temperature," *J. Mater. Sci.*, **24**, 1373–79 (1989).

[25]R. T. Bhatt, "Oxidation Effects on the Mechanical Properties of SiC-Fiber-Reinforced Reaction-Bonded Si_3N_4-Matrix Composites," *J. Am. Ceram. Soc.*, **75**, 406–12 (1992).

[26]J. F. Mandell, D. H. Grande, and J. Jacobs, "Tensile Behaviour of Glass/Ceramic Composite Materials at Elevated Temperatures," *J. Eng. Gas Turbines Power*, **109**, 267–73 (1987).

[27]J. W. Holmes, "Influence of Stress Ratio on the Elevated-Temperature Fatigue of Silicon Carbide Fiber-Reinforced Silicon Nitride Composite," *J. Am. Ceram. Soc.*, **74**, 1639–45 (1991).

[28]J. W. Holmes, "A Technique for Tensile Fatigue and Creep Testing of Fiber-Reinforced Ceramics," *J. Compos. Mater.*, **26**, 915–32 (1992).

[29]A. W. Pryce and P. A. Smith, "Matrix Cracking in Unidirectional Ceramic Matrix Composites under Quasi-Static and Cyclic Loading," *Acta Metall. Mater.*, **41**, 1269–81 (1993).

[30]W. P. Keith and K. T. Kedward, "The Stress–Strain Behavior of a Porous Unidirectional Ceramic Matrix Composite," *Composites*, **26**, 163–74 (1995).

[31]B. F. Sørensen and J. W. Holmes, "Model of the Mechanical Behavior of Continuous Fiber Reinforced Ceramic Matrix Composites During Cyclic Loading," *J. Eur. Ceram. Soc.*, submitted.

[32]T. Mackin and F. W. Zok, "Fiber Bundle Pushout: A Technique for the Measurement of Interfacial Sliding Properties," *J. Am. Ceram. Soc.*, **75**, 3169–71 (1992).

[33]E. Lara-Curzio and M. K. Feber, "Methodology for the Determination of the Interfacial Properties of Brittle Matrix Composites," *J. Mater. Sci.*, **29**, 6152–58 (1994).

[34]B. F. Sørensen and J. W. Holmes, "Effect of Loading Rate on the Monotonic Tensile Behavior and Matrix Cracking of a Fiber-Reinforced Ceramic," *J. Am. Ceram. Soc.*, **79**, 313–20 (1996).

[35]R. W. Goettler and K. T. Faber, "Interfacial Shear Stress in Fiber-Reinforced Glasses," *Compos. Sci. Technol.*, **37**, 129–47 (1989).

[36]B. F. Sørensen and J. W. Holmes, "Fatigue of Continuous Fiber-Reinforced Ceramic Matrix Composites: Review of Mechanisms and Models"; pp. 487–500 in Proceedings of the International Symposium on Fatigue under Thermal and Mechanical Loading. Edited by J. Bressers and L. Remy. Kluwer Academic Publishers, Dordrecht, Netherlands, 1996.

[37]S. M. Spearing, F. M. Zok, and A. G. Evans, "Stress Corrosion Cracking in a Unidirectional Ceramic-Matrix Composite," *J. Am. Ceram. Soc.*, **77**, 562–70 (1994).

[38]B. F. Sørensen and J. W. Holmes, "Influence of Stress Ratio on the Fatigue Life of a Continuous Fiber-Reinforced Ceramic Matrix Composite," unpublished work.

[39]J. W. Holmes, unpublished research.

[40]J. I. Eldridge, "Environmental Effects on Fiber Debonding and Sliding in an SCS-6 SiC Fiber Reinforced Reaction-Bonded Si_3Ni_4 Composite," *Scr. Metall. Mater.*, **32**, 1085–89 (1995).

[41]J. I. Eldridge, R. T. Bhatt, and N. P. Bansal, "Investigation of Fiber/Matrix Interfacial Mechanical Behavior in Ceramic Matrix Composites by Cyclic Fiber Push-in Testing," *Ceram. Eng. Sci. Proc.*, **17**, 266–78 (1996).

[42]W. A. Thomas and J. M. Sanchez, "Influence of Interfacial Sliding Stress on Fatigue Behavior of Oxidized Nicalon/Calcium Aluminosilicate Composites," *J. Am. Ceram. Soc.*, **79**, 2659–65 (1996). □